Laser-induced band-gap collapse in GaAs

E. N. Glezer, Y. Siegal, L. Huang, and E. Mazur
Division of Applied Sciences and Department of Physics, Harvard University, Cambridge, Massachusetts 02138
(Received 11 July 1994; revised manuscript received 7 November 1994)

We present experimentally determined values of the dielectric constant of GaAs at photon energies of 2.2 and 4.4 eV following excitation of the sample with 1.9-eV, 70-fs laser pulses spanning a fluence range from 0 to 2.5 kJ/m^2. The data show that the response of the dielectric constant to the excitation is dominated by changes in the electronic band structure and not by the optical susceptibility of the excited free carriers. The behavior of the dielectric constant indicates a drop in the average bonding-antibonding splitting of GaAs following the laser-pulse excitation. This drop in the average splitting leads to a collapse of the band gap on a picosecond time scale for excitation at fluences near the damage threshold of 1.0 kJ/m^2 and on a subpicosecond time scale at higher excitation fluences. The changes in the electronic band structure result from a combination of electronic screening of the ionic potential as well as structural deformation of the lattice caused by the destabilization of the covalent bonds.

I. INTRODUCTION

Reflectivity and second-harmonic generation studies of femtosecond laser-excited semiconductors show evidence of rapid changes in the material (within a few hundred femtoseconds) following the excitation.[1–6] However, the nature of these material changes cannot be extracted from the results of these experiments. Interpretation of reflectivity and second-harmonic generation results is difficult because these quantities do not directly yield the behavior of intrinsic material properties. In particular, the reflectivity at a specific wavelength, polarization, and incident angle depends on both the real and imaginary parts of the dielectric constant at that wavelength. Furthermore, the measured second-harmonic radiation depends on the dielectric constant at both the fundamental and second-harmonic wavelengths as well as on the second-order susceptibility. The amount of information in the linear reflectivity and second-harmonic generation measurements, therefore, is not sufficient to determine the behavior of the linear or nonlinear optical material properties uniquely.

Without direct determination of the time evolution of the dielectric constant, interpretation of reflectivity and second-harmonic data has relied to date on making assumptions about the functional form of the dielectric constant. Specifically, it has been assumed that changes in the dielectric constant induced by the excitation are dominated by the free-carrier contribution to the optical susceptibility. Under this assumption, the changes in the dielectric constant have been modeled using a Drude-model formalism.[6–8] While this type of assumption is legitimate at lower excitation regimes, it is misleading in the case of laser-induced disordering experiments. Misinterpretation of the data arises because a single-incident-angle reflectivity values does not correspond to a unique value of the dielectric constant. Thus one can reproduce single-incident-angle reflectivity data using dielectric constant values that are completely different from the actual ones.

To avoid relying on an assumed functional form for the dielectric constant in interpreting the results of femtosecond pump-probe experiments on GaAs, we directly determined the time evolution of the real and imaginary parts of the dielectric constant. Specifically, we experimentally determined the behavior of the complex dielectric constant at photon energies of 2.2 and 4.4 eV following excitation with an intense 70-fs pump pulse at 1.9 eV. To uniquely extract the real and imaginary parts of the dielectric constant, two independent measured quantities are necessary. Therefore, at each probe frequency we measured the *p*-polarized reflectivity at two carefully chosen angles of incidence using two simultaneous 70-fs probe beams.[9–11] We then converted each measured pair of reflectivities to the corresponding complex value of the dielectric constant as a function of pump-probe time delay. We verified that our two-angle technique yielded dielectric constant values consistent with reflectivity measurements at a third angle of incidence. The general approach of employing multiparameter optical probing to distinguish Drude and interband contributions to the dielectric constant has been used in other recent work, using ellipsometric techniques.[12–15] The data we present in this paper show that, for excitation fluences greater than 0.5 kJ/m^2, the Drude model does not adequately describe the induced changes to the dielectric constant. The results indicate that changes in the interband transition contribution to the optical susceptibility dominate the behavior of the dielectric constant, as opposed to changes in the free-carrier contribution, as has been generally assumed. This finding implies that the previously observed initial reflectivity rise following high-intensity femtosecond laser-pulse excitation of semiconductors[3–7] is due to large changes in the electronic band structure which result from the excitation.

0163-1829/95/51(11)/6959(12)/$06.00

II. OPTICAL PROPERTIES AND ELECTRONIC STRUCTURE

A. Interband transition contribution to the dielectric function

The interband transition contribution $\chi_{\text{interband}}(\omega)$ to the dielectric function arises from the couplings of states in different bands through the applied electric field. In a direct-gap semiconductor like GaAs, $\chi_{\text{interband}}(\omega)$ is dominated by direct, or vertical, transitions and is therefore closely related to the joint density of states $J(\omega)$ of the material. The joint density of states, in turn, is directly determined by the electronic band structure[16,17]

$$J(\omega)=\sum_{v,c}\frac{2}{(2\pi)^3}\int d^3k\,\delta[\omega_{vc}(\mathbf{k})-\omega]\ , \tag{1}$$

where v and c, respectively, are valence- and conduction-band indices, $\hbar\omega_{vc}$ is the energy separation between band v and band c at a crystal momentum value of $\mathbf{k}$, and the integral is over the Brillouin zone. In the ground state (valence band filled and conduction band empty), the imaginary part of $\chi_{\text{interband}}(\omega)$ approximately satisfies the relation[16,17]

$$\mathrm{Im}[\chi_{\text{interband}}(\omega)]\propto\frac{1}{\omega^2}J(\omega)\ , \tag{2}$$

illustrating the connection between the electronic band structure and the interband transition contribution to the dielectric constant.

Most group-IV and -III-V semiconductors have qualitatively similar joint densities of states, leading to similar dielectric functions in the ground state.[16–18] The solid curves in Fig. 1 show both the real and imaginary parts of the dielectric function of undoped GaAs at room temperature.[19] The three main features labeled E_0, E_1, and E_2 are common to the group-IV and -III-V semiconductors, although their locations and the relative sizes of these features vary from material to material. The point E_0 (at 1.4 eV for GaAs) marks the fundamental band edge below which Im(ε) is zero; E_1 and E_2 [located at 3.0 and 4.75 eV, respectively, for GaAs (Ref. 20)] label the two main absorption peaks in the spectrum. These peaks arise from regions in the band structure (the region around the L point for the E_1 peak and the region around the X point for the E_2 peak—see the GaAs band-structure diagram in Fig. 2) in which the valence band is roughly parallel to the conduction band, resulting in a large joint density of states for direct interband transitions.[16] The E_2 peak, which is roughly coincident with the zero crossing in Re(ε), is the stronger of the two absorption peaks, and its location approximately gives the value of the average bonding-antibonding splitting of GaAs.[17]

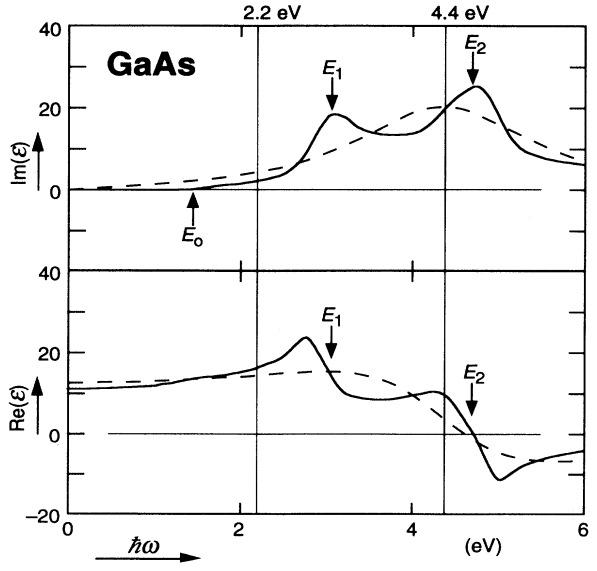

FIG. 1. Dielectric function of GaAs. The solid curves show the dielectric function taken from the literature (see Ref. 19). E_0 labels the fundamental absorption edge, corresponding to the minimum band gap, while E_1 and E_2 label the two main absorption peaks. The dashed curves show a fit of the single-oscillator dielectric function to the solid curves.

In the simplest approximation, the overall shape of the GaAs dielectric function (the solid curves in Fig. 1) resembles that of a charged particle in a damped harmonic-oscillator potential. We can model the GaAs dielectric function as a single average harmonic oscillator with a resonant frequency that corresponds to the average bonding-antibonding splitting,[16] and a width that is related to the spectral range over which the joint density of states is large. The dashed curves in Fig. 1 represent a fit of the single-oscillator dielectric function[21] to the ground-state dielectric function of GaAs. While this type of picture does not describe the structure in the semiconductor dielectric function in detail, it provides a simple physical interpretation for the overall shape and highlights some important characteristics. In particular, it illustrates that the main interband absorption peak in the semiconductor dielectric function has the same features as an oscillator resonance: a zero crossing in the real part coinciding with a peak in the imaginary part. This simplified picture will be helpful in the interpretation of the data presented in Sec. IV.

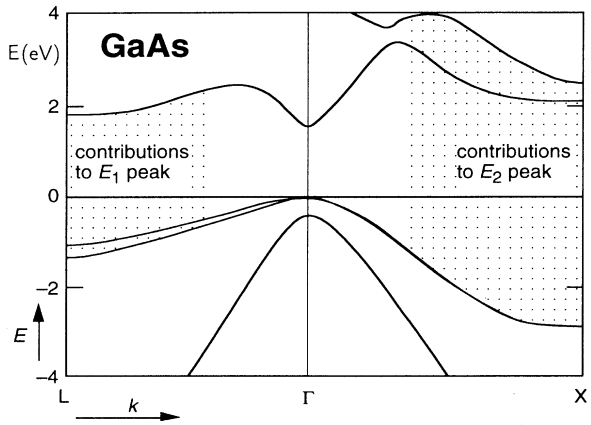

FIG. 2. A section of the electronic band structure of GaAs (see Ref. 17) showing some of the regions that contribute to the E_1 and E_2 absorption peaks in the dielectric function.

B. Free-carrier contribution to the dielectric function—the Drude model

The free-carrier contribution to the dielectric constant of a semiconductor is generally treated in the framework of the Drude model for the ac conductivity of free electrons.[8,22,23] For a semiconductor with a conduction-band electron density of N_e and a valence-band hole density of N_h, the Drude contribution of the free carriers to the optical susceptibility is given by

$$\chi_{\text{Drude}}(\omega)=\frac{ie^2}{\omega}\left[\frac{N_e\tau_e}{m_e^*(1-i\omega\tau_e)}+\frac{N_h\tau_h}{m_h^*(1-i\omega\tau_h)}\right], \quad (3)$$

where e is the charge of the electron, and $m_{e,h}^*$ and $\tau_{e,h}$ are the effective mass and mean collision time of the free electrons and holes. If the free carries are produced by optical excitation, then $N_e=N_h=N$, where N is the number of electron-hole pairs created by the excitation.

The general shape of the Drude optical susceptibility is very different from that of the optical susceptibility near an interband transition resonance. Defining a reduced effective mass m^* such that $1/m^*=1/m_e^*+1/m_h^*$, and assuming that $\tau_e\approx\tau_h\approx\tau$, the real and imaginary parts of $\chi_{\text{Drude}}(\omega)$ are given by

$$\text{Re}[\chi_{\text{Drude}}(\omega)]=-\frac{Ne^2\tau^2}{m^*(1+\omega^2\tau^2)} \quad (4a)$$

and

$$\text{Im}[\chi_{\text{Drude}}(\omega)]=\left[\frac{1}{\omega\tau}\right]\frac{Ne^2\tau^2}{m^*(1+\omega^2\tau^2)}. \quad (4b)$$

Equations (4a) and (4b) show that $\text{Re}[\chi_{\text{Drude}}(\omega)]$ is a featureless, monotonically increasing function of ω, while $\text{Im}[\chi_{\text{Drude}}(\omega)]$ is a featureless, monotonically decreasing function of ω. If $\omega\tau\gg1$, which is generally the case for semiconductors in the visible frequency range, the magnitude of the imaginary part is much smaller than that of the real part, and we can write $\chi_{\text{Drude}}(\omega)\approx-\omega_p^2/4\pi\omega^2$, where $\omega_p\equiv[4\pi Ne^2/m^*]^{1/2}$ is the plasma frequency. The Drude dielectric function $\varepsilon(\omega)=1+4\pi\chi_{\text{Drude}}(\omega)$ goes through a resonance at $\omega=\omega_p$ as $\text{Re}[\varepsilon(\omega)]$ passes through zero. This plasma resonance corresponds to the excitation of plasmons, or collective oscillations of the free-carrier charge density.[24] Note that $\text{Im}[\varepsilon(\omega)]$ continues to decrease as a function of ω at a plasma resonance, in sharp contrast to the peak shape of $\text{Im}[\varepsilon(\omega)]$ at an interband transition resonance. At fixed ω in a semiconductor, one can in principle go through a plasma resonance by increasing the free-carrier density N. In this case, $\text{Re}[\varepsilon(N,\omega)]$ decreases through zero as the carrier density increases, while $\text{Im}[\varepsilon(N,\omega)]$ increases monotonically with carrier density. The contrast between a plasma resonance and an interband transition resonance will further aid in the interpretation of the experimental data in Sec. IV.

C. Standard assumption for $\varepsilon(\omega)$ following laser excitation

As evidenced by changes observed in the reflectivity, excitation of a semiconductor with a laser pulse modifies the dielectric constant of the material.[1–4,8,25–27] The model generally used for the time-dependent dielectric function $\varepsilon(\omega,t)$ of a semiconductor following laser-pulse excitation involves the assumption that the interband contribution to the susceptibility does not change significantly as a result of the excitation: $\chi_{\text{interband}}(\omega,t)\approx\chi_{\text{interband}}(\omega)$.[7,28] Instead, changes in the dielectric function are attributed mainly to the time dependence of $\chi_{\text{Drude}}(\omega,t)$ arising from the time-dependent free-carrier density $N(t)$ produced by the excitation. This model can be expressed as

$$\varepsilon(\omega,t)=1+4\pi\left[\chi_{\text{interband}}(\omega)+\frac{iN(t)e^2\tau}{m^*\omega(1-i\omega\tau)}\right]. \quad (5)$$

The free-carrier density $N(t)$ created by the laser-pulse excitation depends on the excitation fluence ϕ. At a fixed time t after the excitation, $N(\phi,t)$ increases monotonically with excitation fluence. So according to Eq. (5) one would expect $\text{Re}[\varepsilon(\omega,\phi,t)]$ to decrease monotonically and $\text{Im}[\varepsilon(\omega,\phi,t)]$ to increase monotonically with increasing excitation fluence. Furthermore, with $\omega\tau\gg1$, the increase in $\text{Im}[\varepsilon(\omega,\phi,t)]$ should only be slight.

While this Drude-like model for the dielectric constant of a laser-excited semiconductor adequately describes data at low and moderate carrier excitation levels ($N\leq10^{20}$ cm^{-3}),[12,29] the data we present below show that it cannot be used to analyze reflectivity data at high carrier excitation levels ($N\geq10^{21}$ cm^{-3}). The experimental results in Sec. IV indicate that, in this strong excitation regime, the response of the dielectric function to the laser-pulse excitation is dominated by changes in the interband transition contribution to the dielectric constant resulting from a major alteration of the electronic band structure. The difference between the expected behavior of $\varepsilon(\omega,\phi,t)$ based on previous assumptions and the experimentally observed behavior will be highlighted in Sec. IV E.

III. EXPERIMENTAL SETUP

A. Two-color amplified femtosecond laser system

The results presented in this section involve two sets of measurements made using a two-color pump-probe technique. One set consists of data taken using a 70-fs, 1.9-eV pump beam and a simultaneous pair of 70-fs, 2.2-eV probe beams, while the other set consists of data taken using the same pump beam conditions but a doubled probe photon energy of 4.4 eV. To generate pump and probe beams at different frequencies, we pass the amplified output of a colliding pulse mode-locked laser through a 20-mm, single-mode, polarization-preserving optical fiber.[30] Self-phase modulation in the fiber broadens the spectrum of the input pulse from 5 to 200 nm. By splitting this continuum beam with a broadband beamsplitter, we can independently amplify different spectral regions within the 200-nm bandwidth using two separate amplifier chains.[31] A three-stage amplifier using the dye DCM produces a 300-μJ pump beam centered at 635 nm with a 20-nm bandwidth; a two-stage amplifier

using the dye Rhodamine 6G produces a 30-μJ probe beam centered at 570 nm with a 10-nm bandwidth. Both amplifiers are pumped by a frequency-doubled, 10-Hz Nd:YAG (yttrium aluminum garnet) laser. Following amplification, each beam is compressed by a separate grating pair to a 70-fs pulse width [full width at half maximum (FWHM)].

B. Time-resolved determination of the dielectric constant

To determine both the real and imaginary parts of the dielectric constant of GaAs with femtosecond time resolution, we simultaneously measure the reflectivity at two different angles of incidence as a function of pump-probe time delay.[31] In the 2.2-eV experiment, the pair of probe beams is produced simply by splitting the 570-nm beam in two. In the 4.4-eV experiment, we first double the 570-nm beam in a 100-μm-thick BBO crystal before splitting the beam. The probing geometries for both experiments are summarized in Fig. 3. In both cases, the incident beams are polarized in the plane of incidence and are focused onto the same spot on an insulating (110) GaAs wafer (Cr doped, $\rho > 7\times10^7$ Ω cm), which is exposed to air. To monitor a uniformly excited region, we focus the probe beams more tightly than the pump beam: the probed surface area is about 16 times smaller than the 0.01-mm^2 focal area of the pump beam on the sample. Uniform excitation in the probed region is further assured by the smaller penetration depth of the probe beams (between 5 and 170 nm at 2.2 eV and 5 and 10 nm at 4.4 eV) (Ref. 32) compared to that of the pump beam (270 nm). The pump pulse fluence at each pump-probe time delay spans a range from 0 to 2.5 kJ/m^2. The probe beam fluence never exceeds 0.1 kJ/m^2 so as not to produce an detectable changes in the dielectric constant. To avoid cumulative damage effects, we translate the sample during data collection so that each data point is obtained at another spot on the sample.

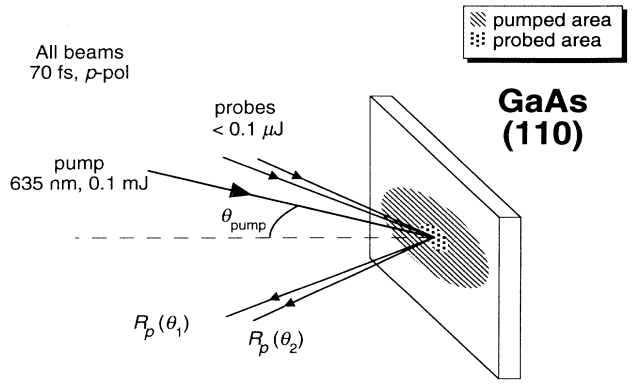

probe wavelength	θ_1	θ_2	θ_{pump}
570 nm (2.2 eV)	70.9°	75.8°	63°
285nm (4.4 eV)	58.5°	76.0°	68°

FIG. 3. Probing geometry and incident angles for the 2.2- and 4.4-eV measurements. All beams are p polarized.

We convert each pair of reflectivity measurements to the corresponding real and imaginary parts of the dielectric constant by numerically inverting the Fresnel formula for reflectivity as a function of the incident angle. Setting one of the probe beam angles of incidence to the Brewster angle provides good sensitivity in distinguishing changes in Re(ε) from changes in Im(ε) because the p-polarized reflectivity at this angle is determined mainly by Im(ε).[33] We base our choice of the second incident angle, which is not as critical, on constraints in the experimental setup. The two angles of incidence for the 2.2-eV measurements were 75.8° and 70.9°; in the 4.4-eV measurements we used 76.0° and 58.5°. To keep the angular separation between pump and probes small, we used a 63° incident angle for the p-polarized pump beam in the 2.2-eV experiment, and a 68° incident angle in the 4.4-eV experiment.

Because the GaAs surface oxidizes in air, we use a three-phase model (air-oxide-GaAs) in converting the reflectivity data to values for the dielectric constant. Surface roughness effects can be accounted for in this model by adjusting the effective thickness of the oxide layer.[34] We calibrated the effective thickness of the oxide layer by measuring reflectivity as a function of incident angle in the absence of excitation by a pump pulse. Using the ground-state dielectric constant of GaAs,[19] and a value of $\varepsilon=4$ for the dielectric constant of the oxide layer,[34] we fit the three-phase model to the measured angle dependence with the effective oxide layer thickness as a fit parameter. This procedure consistently yielded an effective thickness for the oxide layer of about 4 nm. In the 2.2-eV experiment the obtained value was 4.2 ± 0.4 nm, while in the 4.4-eV experiment the value was 4.4 ± 0.4 nm.

As a consistency check of our determination of the dielectric constant, we measured the time evolution of the reflectivity at a third, completely different, angle of incidence (45° for the 2.2-eV case and 35.5° for the 4.4-eV case) under similar pump pulse excitation conditions at both probe frequencies. We then calculated the expected reflectivity at that third incident angle using our experimentally determined time- and fluence-dependent values for the dielectric constant. The measured reflectivity showed excellent agreement with the calculated reflectivity at this third angle of incidence for both the 2.2- and 4.4-eV data. An example of this consistency check is shown in Sec. IV E (see Fig. 11).

IV. EXPERIMENTAL RESULTS

A. Dielectric constant at 2.2 eV

Figures 4 and 5 summarize the experimental data for the dielectric constant at 2.2 eV. In Fig. 4, Re(ε) (filled circles) and Im(ε) (open circles) are plotted vs pump-probe time delay for four different excitation fluences; in Fig. 5, Re(ε) and Im(ε) are plotted vs pump fluence at four different time delays. The change induced in the dielectric constant by the pump pulse excitation is completely different from that expected from the free-carrier contribution to the optical susceptibility. At pump fluences near 1 kJ/m^2, Im(ε) starts at an initial value of

about 2, rises to a peak near 60, and then drops to somewhere between 10 and 15—a strong contrast to the slight, featureless increase predicted by the Drude model. Re(ε), meanwhile, initially decreases slightly but then sharply increases before dropping through zero. Note that the zero crossing of Re(ε) roughly coincides with the peak in Im(ε).

The results shown in Figs. 4 and 5 indicate that a strong absorption peak comes into resonance with the probe frequency as a result of the excitation. The resonance behavior is most striking in Fig. 5 because the features are particularly clear when plotted versus pump fluence. This behavior must result from an interband absorption peak and not from a free-carrier plasma resonance because the zero crossing in Re(ε) is accompanied by a peak in Im(ε) rather than by a steady increase. From the behavior of Re(ε), we can infer the time evolution of this interband absorption peak. Because Re(ε) is initially positive, the resonant frequency of the observed absorption peak evidently starts out higher than the probe frequency; it then sweeps down through the probe frequency as Re(ε) drops through zero.

The rate at which the resonant frequency of the absorption peak drops through the probe frequency depends on the strength of the excitation: the higher the pump fluence, the faster Re(ε) drops through zero. Figure 6 illustrates this dependence by showing the time de-

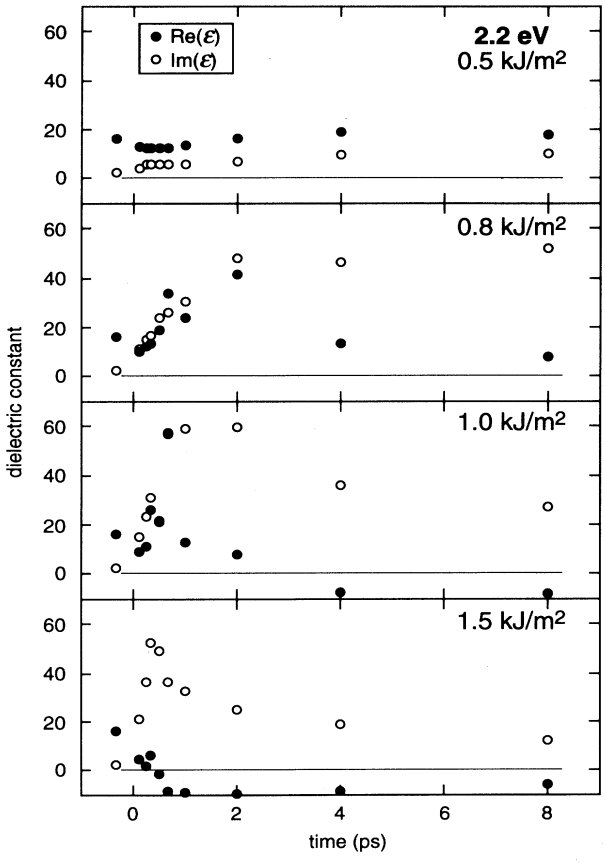

FIG. 4. Dielectric constant at 2.2 eV vs pump-probe time delay for four different pump fluences ●: Re(ε); ○: Im(ε).

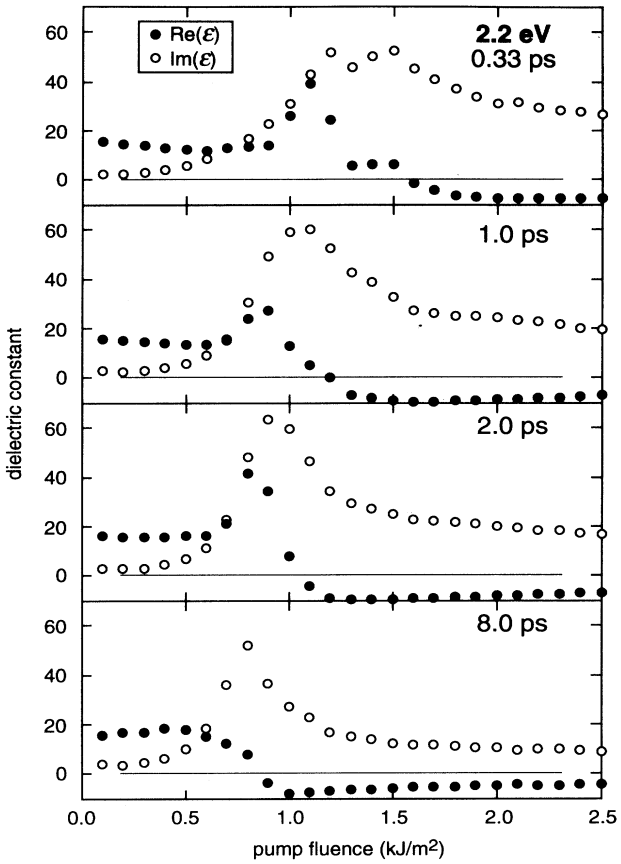

FIG. 5. Dielectric constant at 2.2 eV vs pump fluence for four different pump-probe time delays. ●: Re(ε); ○: Im(ε).

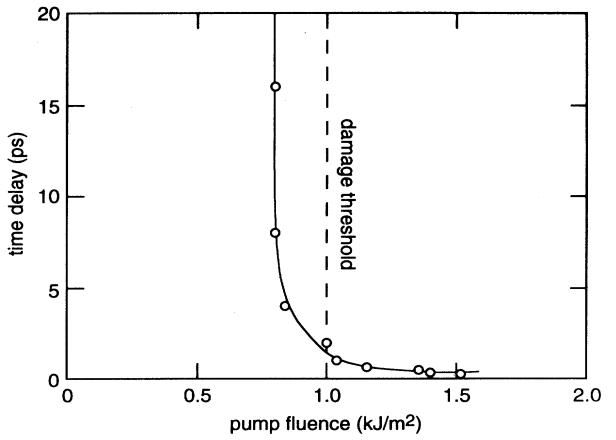

FIG. 6. Pump-probe time delays at which Re(ε)=0 for different pump fluences. The solid curve is drawn to guide the eye, and the dashed line corresponds to the damage threshold of 1.0 kJ/m^2. At fluences above this value the induced changes in the material are irreversible, while at fluences below the damage threshold the induced changes are reversible.

lay at which Re(ε) crosses through zero plotted vs pump fluence. For fluences around 2.0 kJ/m^2, the absorption peak comes into resonance with the probe frequency within a few hundred femtoseconds; at fluences just above 0.8 kJ/m^2, on the other hand, the absorption peak takes on the order of 10 ps to come into resonance. For fluences below 0.8 kJ/m^2, Re(ε) never goes through zero, indicating that the excitation is not strong enough to bring the resonant frequency of the peak down to the probe frequency.

The dashed line in Fig. 6 at 1.0 kJ/m^2 indicates the threshold fluence for permanent damage to the sample. We determined this threshold by correlating pump pulse fluence with the size of damage spots on the sample measured through a microscope. Above the damage threshold the pump pulse induces irreversible changes in the sample, while below the damage threshold the induced changes are reversible. Measurements taken several seconds after the excitation confirm that the dielectric constant eventually returns to its initial value for fluences below the damage threshold. Note, however, that the absorption peak comes into resonance with the probe frequency even for pump fluences below this damage threshold.

The use of the Fresnel equations to extract the dielectric constant from reflectivity measurements presumes the existence of a sharp boundary between two different media. While this assumption is clearly justified below the damage threshold, at higher fluences density gradients can develop due to hydrodynamic expansion at the surface.[13] Furthermore, the hydrodynamic expansion can lead to the formation of an absorptive cloud, accompanied by nonspecular scattering of the probe light. The formation of such an absorptive cloud has been seen in silicon, beginning at about 10 ps after excitation by a pulse with fluence above five times greater than the damage threshold.[2] In GaAs, a decrease in the specular reflectivity and the onset of nonspecular scattering of the probe light, also beginning about 10 ps after the excitation, has been observed above the damage threshold.[27] To remain within the validity range of the sharp boundary assumption, we limit the range of time delays over which we extract the dielectric constant to 8 ps. By measuring the reflectivity at a third angle for both 2.2- and 4.4-eV experiments, we verified that the Fresnel equations are indeed valid over our entire experimental range.

B. Qualitative picture—band-gap collapse

It is useful at this point to develop a qualitative interpretation of the data presented in Sec. IV A; a more quantitative analysis of the results will appear in Sec. IV D. The first step in interpreting the data is to attach a physical significance to the interband absorption peak. As discussed in Sec. II A, the dielectric function of GaAs can be approximated by that of a damped single harmonic oscillator with a resonant frequency equal to the average bonding-antibonding splitting.[16] Identifying the interband absorption peak in the data with the harmonic-oscillator absorption peak, we can think of the shift in this peak as a drop in the average bonding-antibonding splitting. In GaAs, the average bonding-antibonding splitting in the ground state is about 4.75 eV.[17,20] The 2.2-eV data then indicate that the laser-pulse excitation induces a drop in the average bonding-antibonding splitting from 4.75 to below 2.2 eV. Note that this drop in the average splitting by more than a factor of 2 occurs even for fluences below the damage threshold, an excitation regime in which the induced changes are reversible.

Figure 7 illustrates schematically the qualitative picture that emerges from the 2.2-eV data. The average bonding-antibonding splitting ΔE_{b-a} starts out far above 2.2 eV, so the probe photon energy lies at the foot of the single-oscillator absorption peak where Im(ε) is small (step 1 in Fig. 7). As a result of the excitation in step 1, ΔE_{b-a} begins to decrease, leading to a downward shift in the resonant frequency of the single-oscillator absorption peak and therefore a rise in Im(ε) at 2.2 eV (step 2 in Fig. 7).[35] As ΔE_{b-a} drops past 2.2 eV (step 3 in Fig. 7), Im(ε) goes through a peak. If ΔE_{b-a} drops far enough, the minimum in the conduction band will drop below the maximum in the valence band, and the semiconductor will take on metallic properties (step 4 in Fig. 7). The 2.2-eV dielectric constant at high fluences and long-time delays, after the collapse of the band gap, is consistent with the characteristics of a poor metal and is similar to that of liquid silicon[22] and liquid carbon[26] produced by laser-pulse-excitation.

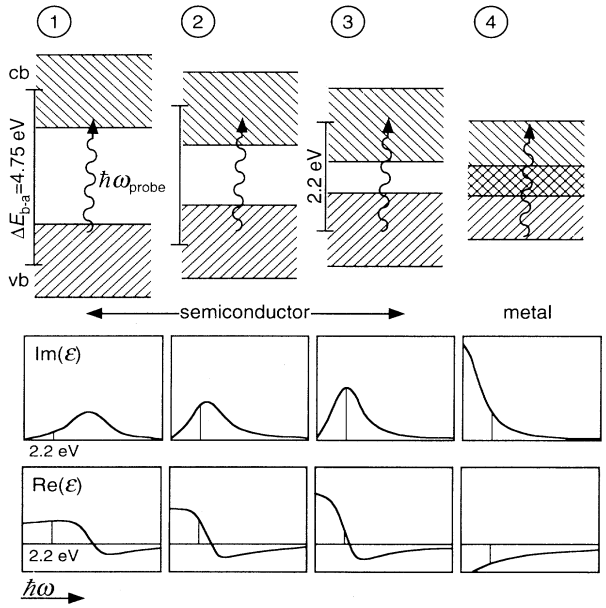

FIG. 7. Schematic representation of the band-gap collapse. The pump pulse leads to a drop in the average bonding-antibonding splitting from its initial value of about 4.75 eV to below the probe photon energy of 2.2 eV. If the minimum in the conduction band drops below the maximum in the valence band, the material takes on metallic properties. The drop in average bonding-antibonding splitting appears as a shift in the main absorption peak in the dielectric function, as illustrated in the figure. cb: conduction band; vb: valence band; ΔE_{b-a}: average bonding-antibonding splitting; $\hbar\omega_{probe}$: probe photon energy.

This interpretation of the 2.2-eV data in terms of a drop in the average bonding-antibonding splitting allows us to predict qualitatively the behavior of the dielectric constant at different photon energies under similar excitation conditions. In particular, for a given excitation strength, the dielectric constant at a probe photon energy between 2.2 and 4.75 eV should exhibit resonance features at an earlier pump-probe time delay than the dielectric constant at 2.2 eV. Equivalently, for a fixed pump-probe time delay, the dielectric constant at a probe photon energy in the above range should exhibit resonance features at a lower pump fluence than the dielectric constant at 2.2 eV.

C. Dielectric constant at 4.4 eV

To verify the interpretation described in Sec. IV B, we measured the behavior of the dielectric constant at 4.4 eV, which is only slightly below the initial value of the average bonding-antibonding splitting of GaAs. Figures 8 and 9 summarize the data at 4.4 eV. Figure 8 presents the time dependence of the 4.4-eV dielectric constant at the same four pump fluences shown in Fig. 4, and Fig. 9 shows the fluence dependence of the 4.4-eV dielectric constant for fixed pump-probe time delays. Note that at equal pump fluence the peak in Im(ε) and the zero crossing in Re(ε) occur at earlier time delays in the 4.4-eV case than in the 2.2-eV case. Correspondingly, these features occur at lower fluences in the 4.4-eV data than in the 2.2-eV data for equivalent time delays. This behavior stands out in Fig. 10, which adds to Fig. 6 the corresponding points for the 4.4-eV results. Re(ε) at 4.4 eV

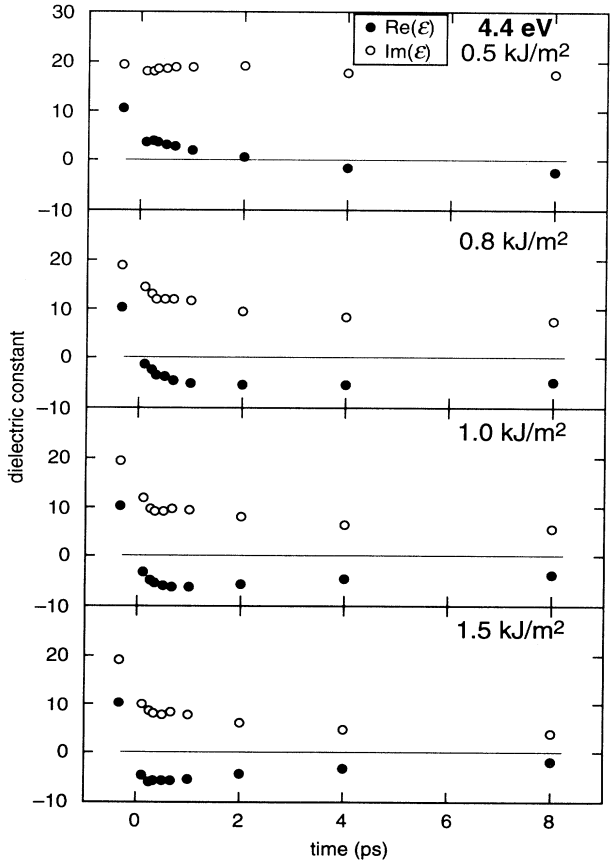

FIG. 8. Dielectric constant at 4.4 eV vs pump-probe time delay for four different pump fluences. ●: Re(ε); ○: Im(ε).

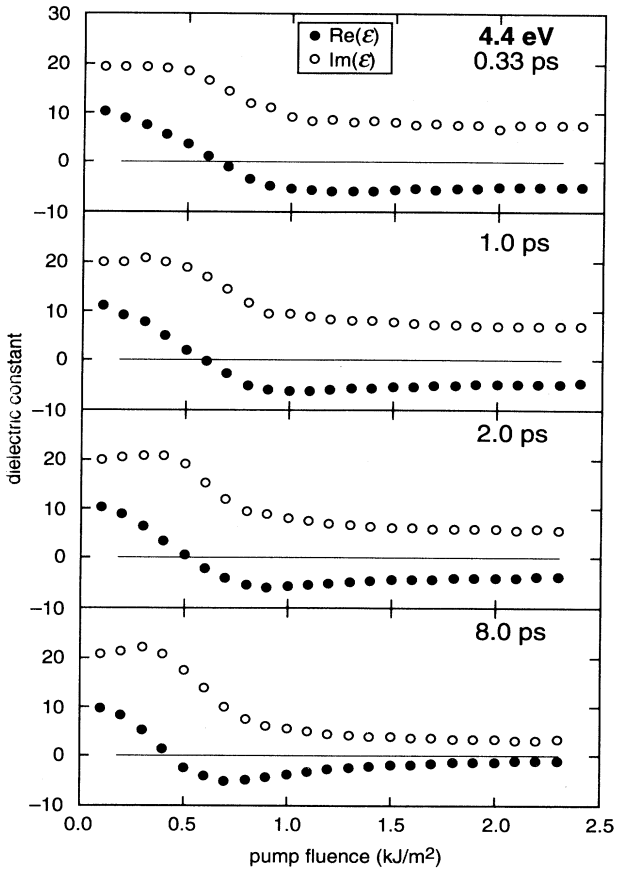

FIG. 9. Dielectric constant at 4.4 eV vs pump fluence for four different pump-probe time delays. ●: Re(ε); ○: Im(ε).

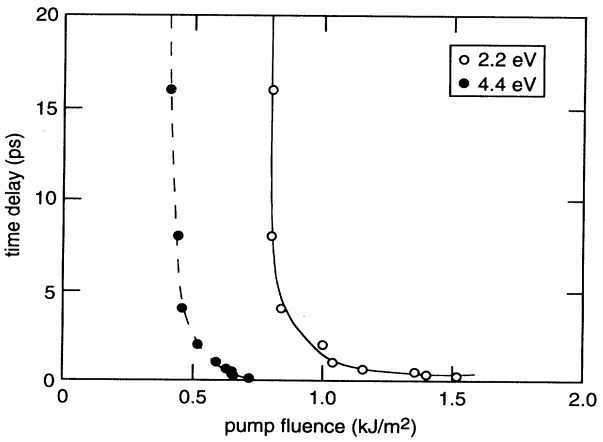

FIG. 10. Pump-probe time delays at which Re(ε)=0 for different pump fluences at both 2.2 and 4.4 eV. The curves are drawn to guide the eye. ●: 4.4 eV; ○: 2.2 eV.

crosses zero for fluences as low as 0.5 kJ/m^2 compared to the minimum fluence of 0.8 kJ/m^2 required for a zero crossing at 2.2 eV.

The behavior of the dielectric constant at 4.4 eV is indeed consistent with the picture described in Sec. IV B of a drop in the average bonding-antibonding splitting. Following the pump pulse excitation, ΔE_{b-a} drops from its initial value of about 4.75 eV first past 4.4 eV, and then continues down past 2.2 eV. A stronger excitation causes a faster drop through both probe frequencies. At pump fluences between 0.5 and 0.8 kJ/m^2, the excitation is strong enough to bring the resonant frequency of the absorption peak below 4.4 eV but not all the way down to 2.2 eV. Note that since 4.4 eV is close to the initial value of the average bonding-antibonding splitting, Im[ε(4.4 eV)] does not rise much above its initial value before coming down.

D. The role of free-carrier contributions

The striking resonance behavior we observe indicates that the response of the dielectric constant to the excitation is dominated by changes in the electronic band structure rather than by free-carrier contributions the optical susceptibility. However, this does not mean that the free-carrier contributions are absent. One can get a sense of the size of these contributions to the optical susceptibility by looking at low fluence data, where the band-structure changes are not strong enough to overwhelm the free-carrier effects. At 0.5 kJ/m^2, for example, Re(ε) at 2.2 eV shows an initial decrease within a few hundred femtoseconds and then recovers on a picosecond time scale (see top graph in Fig. 4). This behavior is consistent with the expected effect of the optical susceptibility of the excited free carriers on Re(ε).[37] According to Eq. (4a), the initial creation of free carriers by the pump pulse should be accompanied by a negative contribution to Re(ε). As the free-carrier population decreases due to strong Auger recombination, the magnitude of the free-carrier contribution decreases and Re(ε) recovers. The observed recovery time of a few picoseconds agrees with the predicted high carrier-density Auger recombination time predicted by Yoffa.[38] However, even at 0.5 kJ/m^2, the changes in the interband transition contribution are already large enough to affect the dielectric constant at 2.2 eV, as evidenced by the behavior of Im(ε), which shows no recovery on a picosecond time scale. At fluences exceeding 0.6 kJ/m^2, the interband transition resonance behavior at 2.2 eV is so strong that it masks the free-carrier contributions to the dielectric constant.

E. Comparison of observed behavior with expected behavior

Figure 11 highlights the unexpected nature of the experimental results by comparing the observed behavior of the dielectric constant with that expected based on the standard assumption expressed in Eq. (5). This figure also illustrates the ambiguity inherent in the interpretation of single-angle-of-incidence reflectivity measurements. The top graph in Fig. 11(a) shows the experimentally determined dielectric constant at 2.2 eV plotted against pump fluence at a time delay of 2 ps (this corresponds to the third graph in Fig. 5). The dielectric constant values in this graph are used to calculate the corresponding p-polarized reflectivity at an incident angle of 45°, shown by the curve in the bottom graph in Fig. 11(a). This curve agrees with the experimental values of the 45° p-reflectivity also measured at a time delay of 2 ps and represented by the open squares in the graph. Figure 11(a) therefore provides a consistency check for our two-angle technique. For comparison, Fig. 11(b) presents in the top graph a Drude-like dielectric constants based on Eq. (5), without the restriction $\omega\tau \gg 1$, that is chosen also to reproduce the measured 45°-reflectivity values, as seen in the bottom graph. It is important to emphasize that the distinctive resonance features of the actual, experimentally determined dielectric constant in Fig. 11(a) produce the same reflectivity values at 45° incidence as the Drude-like behavior of the computer-generated, but in-

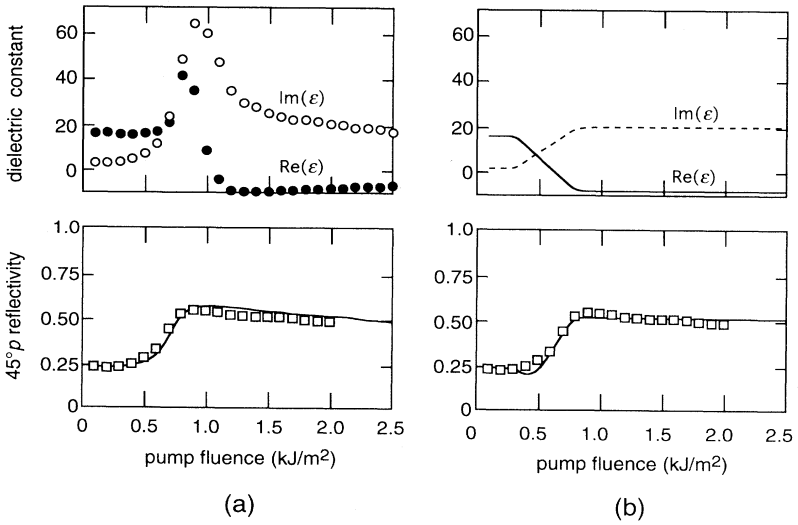

FIG. 11. Comparison of observed behavior with expected behavior at a time delay of 2 ps. (a) Top graph shows experimentally determined values for the 2.2-eV dielectric constant. ●: Re(ε); ○: Im(ε). (b) Top graph shows the computer-generated, Drude-like dielectric constant chosen to reproduce the measured reflectivity. ——: Re(ε); — — —: Im(ε). In both (a) and (b), the bottom graph shows the p-polarized reflectivity at 45° incident angle. ——: reflectivity calculated from dielectric constant; □: measured reflectivity.

correct, dielectric constant in Fig. 11(b). However, the two dielectric constants reflect very different underlying physics: changes in $\chi_{\text{interband}}(\omega)$ dominate the former, while the latter would indicate the prevalence of changes in $\chi_{\text{Drude}}(\omega)$. Thus experimental determination of the complex dielectric constant is essential to understanding laser-induced phase transitions in semiconductors.

V. ANALYSIS AND DISCUSSION

A. Quantitative analysis—double-oscillator model

To refine the qualitative picture we have so far developed of a laser-induced drop in the average bonding-antibonding splitting,[9] we can use a damped double-oscillator model that better captures the features of the ground-state dielectric function of GaAs. The double-oscillator dielectric function is given by the expression

$$\varepsilon(\omega)=1+\omega_p^2\left[\frac{f_1}{(\omega_1^2-\omega^2+i\omega\Gamma_1)}+\frac{f_2}{(\omega_2^2-\omega^2+i\omega\Gamma_2)}\right], \tag{6}$$

where ω_i and Γ_i are the resonant frequency and the spectral width of the ith oscillator. The oscillator strength f_i, which obeys the sum rule $f_1+f_2=1$, corresponds to the fraction of the total number of electrons N (appearing in ω_p^2) that contributes to the strength of the ith oscillator. Fitting Eq. (6) to the GaAs ground-state dielectric function[19] using $\hbar\omega_1=3.10$ eV and $\hbar\omega_2=4.75$ eV to match the location of the E_1 and E_2 absorption peaks yields $\hbar\Gamma_1=1.6$ eV, $\hbar\Gamma_2=0.68$ eV, $\hbar\omega_p=13.7$ eV, $f_1=0.16$, and $f_2=0.84$. The higher value of f_2 compared to f_1 indicates that a larger region of the band structure contributes to the E_2 peak than to the E_1 peak.

To model the response of the dielectric function to the laser-pulse excitation using the double-oscillator model, we fit Eq. (6) simultaneously to the real and imaginary parts of the dielectric constant at both 2.2 and 4.4 eV for each pump fluence and time delay. The fit parameters here are ω_1, ω_2, Γ_1, and Γ_2 (ω_p, f_1, and f_2 are held constant), implying that both the location and the width of each of the two absorption peaks can vary as a result of the excitation. To ensure reasonable fluence and time evolution of the parameters, we impose the additional constraint when fitting Eq. (6) to the data that each parameter not change too much for each subsequent fluence or time step. For measurements taken at a pump-probe time delay of -0.33 ps, before the pump pulse arrives that the sample, the double-oscillator fit to the data produces values of $\hbar\omega_1=3.10$ eV, $\hbar\omega_2=4.77$ eV, $\hbar\Gamma_1=1.9$ eV, and $\hbar\Gamma_2=0.73$ eV, closely reproducing the ground-state dielectric function (see top graphs in Fig. 12). This result for negative pump-probe time delay provides a consistency check for the double-oscillator fitting routine.

Figure 12 shows the time evolution of the full double-oscillator dielectric function (plotted versus photon energy) for excitation with a pump fluence of 1.0 kJ/m^2. As seen in the figure, the double-oscillator model fits the observed values of the complex dielectric constant at both 2.2 and 4.4 eV very well. The fitting results at other pump fluences are in similar agreement with the data. The most interesting aspect of the time evolution of the dielectric function shown in Fig. 12 is that it initially exhibits primarily a broadening of the absorption peaks followed by a shift to lower photon energy in the location of the resonance features.

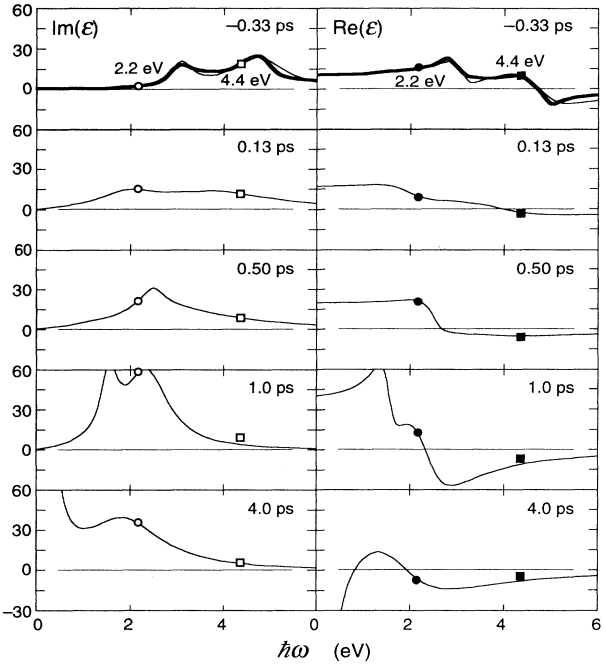

FIG. 12. Time evolution of double-oscillator model dielectric function vs photon energy for excitation with a pump fluence of 1.0 kJ/m^2. Thicker curves in the top graphs show the dielectric function of GaAs from the literature (see Ref. 19). The data points are experiment values at 2.2 and 4.4 eV. ○: Im(ε) at 2.2 eV; □: Im(ε) at 4.4 eV; ●: Re(ε) at 2.2 eV; ■: Re(ε) at 4.4 eV.

We can interpret the plots in Fig. 12 in terms of the electronic band structure of GaAs (see Fig. 2). The initial broadening and shift of the absorption peaks may result from the valence and conduction bands becoming less parallel in the regions around the L and X points, which contribute, respectively to the E_1 and E_2 peaks. Such an effect would occur, for example, if the direct gap at the X point became significantly smaller while the direct gap at the Γ point did not. The subsequent narrowing of the absorption peaks as they continue to slide to even lower photon energies suggests that as parts of the valence and conduction bands grow closer together, they also become more parallel. This type of behavior could arise, for instance, from the region between the L point and the Γ point if the direct gap at the L point decreased from its initial value of about 3 eV while the direct gap at the Γ point continued to remain roughly the same at about 1.4 eV. The behavior of $\varepsilon(\omega)$ near $\omega=0$ (infrared frequencies) at a pump-probe time delay of 4.0 ps, reminiscent of the infrared spectrum of metals, is consistent with a collapse of the minimum band gap. The large, positive

values of Im(ε) and large, negative values of Re(ε) in this frequency range develop as the resonant frequency of one of the absorption peaks approaches zero. Once the minimum band gap goes to zero, one would indeed expect a resonance at $\omega=0$.

It is important to note that we fit the four-parameter double-oscillator model to just four independent values [Re(ε) and Im(ε) at 2.2 and 4.4 eV] at each pump fluence and time delay. Thus, while the experimental data presented in Sec. IV strongly indicate significant band-structure changes marked by a drop in the average bonding-antibonding splitting, the details of these changes are not uniquely determined by the double-oscillator model analysis. Further refinement of our picture of the laser-induced changes in the electronic band structure requires an experimental determination of the dielectric function over a wide range of probe photon energies rather than at a few discrete points. To this end, we are currently developing a broadband probe as well as incorporating broadband light detection capabilities into the two-angle reflectivity technique. We should stress, however, that although we do not currently know all of the details, the data presented in this paper conclusively show that intense femtosecond laser-pulse excitation of GAs leads to a major change in the electronic band structure marked by a drop in the average separation between the valence and conduction bands.

B. Underlying physics—electronic screening and structural change

What underlying physical effects are responsible for this alteration of the band structure? To answer this question, we should examine two main sources of band-structure modification: electronic screening and structural change. Through electron-hole pair generation, the pump pulse creates a large population of mobile charge carriers that can partially screen the ionic potential in the material. Since the average bonding-antibonding splitting increases with the strength of the ionic potential,[17] electronic screening reduces the average bonding-antibonding splitting. Note that electronic screening, through its modification of the band structure, changes the interband transition contribution to the dielectric constant and is therefore completely different from the direct intraband contribution of the free carriers to the dielectric constant through a Drude term. A recent calculation shows that when 10% of the valence electrons are excited to the conduction band, the direct gap at the X point in the band structure of GaAs will decrease by roughly 2 eV due to electronic screening and many-body band-gap renormalization, while the direct gap at the Γ point changes only slightly.[39] Such an effect would lead to an immediate broadening and shift of the absorption peaks in the dielectric function, as discussed in Sec. V A.

Because the strength of electronic screening increases with the free-carrier density, the effects due to screening should follow the carried density instantaneously. Therefore, the effect of screening on the dielectric constant should be largest when the free-carrier density is highest—i.e., immediately following the excitation. As Auger recombination and diffusion reduce the free-carrier density, the influence of electronic screening on the band structure should correspondingly decrease. The time scale for electronic screening is consistent with that for the initial broadening of the absorption peaks, seen in Fig. 12 at the earliest time delays. However, the subsequent changes in the dielectric constant, marked primarily by a shift in the resonance features, continue to grow with time delay during the picoseconds following the excitation, when the carrier density is already decreasing from its peak value. Electronic screening by itself, therefore, cannot explain all of the observed behavior.

To account for the time evolution of the shift in the resonance features of the dielectric constant, we must examine the effect of lattice structural change on the band structure. The electronic band structure is determined by the crystal structure. The semiconducting behavior of group-IV and -III-V material such as GaAs arises from the tetrahedrally coordinated diamond or zinc-blende arrangement of the constituent atoms. If this arrangement is disturbed, the electronic properties will change accordingly. In general, deformation of the diamond or zinc-blende structure leads to a collapse of the band gap and a semiconductor-metal transition.[17,40–42] Just a 10% change in average bond length is enough to cause a semiconductor-metal transition.[42] Note that an ionic velocity as small as 25 m/s is already sufficient to achieve a 10% change in the GaAs bond length within 1 ps.

Because the covalent bonds of semiconductors like GaAs are stabilized by the valence electrons, excitation of a sufficient number of electrons from bonding valence states to antibonding conduction states can lead directly to lattice instability.[43–45] If the femtosecond pump pulse is intense enough to excite this critical density of electrons, the resulting instability in the lattice will cause the atoms to move toward a new minimum-potential-energy configuration. This deformation of the lattice begins immediately following the excitation but continues long after the incidence of the pump pulse. The change in the dielectric constant accompanying the lattice deformation should therefore continue to increase in the picoseconds following the excitation, in agreement with the observed behavior of the dielectric constant.

Note that even below the damage threshold, in the fluence range of 0.8–1.0 kJ/m^2, the laser-pulse excitation induces a drop in the average bonding-antibonding splitting from 4.75 eV down to 2.2 eV within 8 ps. This suggests that reversible structural change takes place below the permanent damage threshold. The changes in the optical properties are considerably greater than those that could result from lattice heating, even up to the melting temperature of 1511 K. The effect of lattice heating on the dielectric constant has been observed at much lower excitation fluences (10^{-3} kJ/m^2) in Ge and $Si_{1-x}Ge_x$ alloys.[12] Based on the temperature dependence of the optical properties of silicon,[46] heating from 10 K up to 1000 K results in about a 0.4-eV decrease in the average optical gap. This decrease is linear with temperature above roughly 200 K. Similar temperature dependence has been measured in GaAs, although only up to 300 K, by Walter *et al.*[47] It is quite unlikely that even near the

melting temperature the average bonding-antibonding splitting would drop down to 2.2 eV. Finally, the observed resonance in the 0.8–1.0-kJ/m^2 fluence range is very similar to that observed above 1.0 kJ/m^2, only slower, indicating that even below the damage threshold the underlying cause for the drop in the splitting is structural change. The value of 0.8 kJ/m^2 does not represent a fundamental threshold, but is simply the lowest fluence that brings the bonding-antibonding splitting into resonance with the 2.2-eV probe frequency within 8 ps.

Below an excitation fluence of 0.8 kJ/m^2 it is more difficult to identify the source of the observed changes in optical properties. For example, at 0.5-kJ/m^2 excitation (Fig. 4, top graph), we see that the imaginary part of the 2.2-eV dielectric constant has not recovered after 8 ps. Even more pronounced is the drop in the real part of the dielectric constant at 4.4 eV, which also does not recover by 8 ps (Fig. 8, top graph). These persistent effects are due to changes in the band structure, and correspond to a downward shift and broadening of the resonant features in the dielectric spectrum. The source of these changes may be lattice heating (thermal motion of the ions), structural change (a deformation of the lattice structure), or a combination of the two.

VI. CONCLUSION

Our data show that a Drude model cannot be used to analyze high-intensity femtosecond pump-probe reflectivity measurements. At pump fluences greater than 0.5 kJ/m^2, the excitation causes major changes in the electronic band structure. Because of these changes, the behavior of $\chi_{\text{interband}}(\omega)$ rather than $\chi_{\text{Drude}}(\omega)$ dominates the response of the dielectric constant to the excitation.

The data indicate that the femtosecond laser-pulse excitation induces a drop in the average bonding-antibonding splitting. This drop manifests itself in a decrease in frequency of the main absorption resonances in the GaAs dielectric function. The rate and extent of the drop in average splitting increase with pump fluence. At fluences between 0.8 and 1.0 kJ/m^2, the average splitting drops reversibly by more than a factor of 2. If the average splitting decreases enough, the minimum in the conduction band drops below the maximum in the valence band, resulting in metallic behavior. Electronic screening may account for the initial changes in the dielectric function, consisting primarily of a broadening of the absorption peaks, while the subsequent shift in the resonance features most likely results from lattice deformation caused by destabilization of the covalent bonds.

ACKNOWLEDGMENTS

We appreciate many useful discussion with Professor N. Bloembergen, Professor H. Ehrenreich, and Professor E. Kaxiras. E.N.G. gratefully acknowledges support from the Fannie and John Hertz foundation. This work was supported by Contract Nos. ONR N00014-89-J-1023 and NSF DMR 89-20490.

[1]C. V. Shank, R. Yen, and C. Hirlimann, Phys. Rev. Lett. **51**, 900 (1983).

[2]M. C. Downer, R. L. Fork, and C. V. Shank, J. Opt. Soc. Am. B **2**, 595 (1985).

[3]H. W. K. Tom, G. D. Aumiller, and C. H. Brito-Cruz, Phys. Rev. Lett. **60**, 1438 (1988).

[4]S. V. Govorkov, I. L. Shumay, W. Rudolph, and T. Schroeder, Opt. Lett. **16**, 1013 (1991).

[5]K. Sokolowski-Tinten, H. Schulz, J. Bialkowski, and D. von der Linde, Appl. Phys. A **53**, 227 (1991).

[6]P. N. Saeta, J. Wang, Y. Siegal, N. Bloembergen, and E. Mazur, Phys. Rev. Lett. **67**, 1023 (1991).

[7]C. V. Shank, R. Yen, and C. Hirlimann, Phys. Rev. Lett. **50**, 454 (1983).

[8]H. Kurz and N. Bloembergen, in *Energy Beam-Solid Interactions and Transient Thermal Processing,* edited by D. K. Biegelsen, G. A. Rozgonyi, and C. V. Shank (Materials Research Society, Pittsburgh, 1985).

[9]Y. Siegal, E. N. Glezer, and E. Mazur, Phys. Rev. B **49**, 16 403 (1994).

[10]Y. Siegal, E. N. Glezer, and E. Mazur, in *Femtosecond Chemistry,* edited by J. Manz and L. Wöste (Verlag Chemie, Berlin, 1994).

[11]Y. Siegal, E. N. Glezer, L. Huang, and E. Mazur, in *Ultrafast Phenomena in Semiconductors,* edited by D. K. Ferry and H. M. van Driel (SPIE, Bellingham, WA, 1994).

[12]H. R. Choo, X. F. Hu, and M. C. Downer, Appl. Phys. Lett. **63**, 1507 (1993).

[13]X. Y. Wang and M. C. Downer, Opt. Lett. **17**, 1450 (1992).

[14]M. C. Downer, H. Ahn, D. H. Reitze, and X. Y. Wang, Int. J. Thermophys. **14**, 361 (1993).

[15]H. Ahn, X. Y. Wang, and M. C. Downer, in *Short Wavelength V: Physics with Intense Laser Pulses,* edited by M. D. Perry and P. B. Corkum (Optical Society of America, Washington, D.C., 1993).

[16]M. L. Cohen and J. R. Chelikowsky, *Electronic Structure and Optical Properties of Semiconductors* (Springer-Verlag, Berlin, 1988).

[17]W. A. Harrison, *Electronic Structure and the Properties of Solids: The Physics of the Chemical Bond* (Dover, New York, 1989).

[18]H. R. Philipp and H. Ehrenreich, Phys. Rev. **129**, 1550 (1963).

[19]E. D. Palik, in *Handbook of Optical Constants of Solids,* edited by E. D. Palik (Academic, New York, 1985).

[20]D. E. Aspnes, G. P. Schwartz, G. J. Gualtieri, A. A. Studna, and B. Schwartz, J. Electrochem. Soc. **128**, 590 (1981).

[21]J. D. Jackson, *Classical Electrodynamics* (Wiley, New York, 1975).

[22]P. M. Fauchet and K. D. Li, J. Non-Cryst. Solids **97&98**, 1267 (1987).

[23]H. M. van Driel, Phys. Rev. B **35**, 8166 (1987).

[24]N. W. Ashcroft and N. D. Mermin, *Solid State Physics* (Saunders College, Philadelphia, 1976).

[25]J. M. Liu, A. M. Malvezzi, and N. Bloembergen, in *Energy*

Beam-Solid Interactions and Transient Thermal Processing, edited by D. K. Biegelsen, G. A. Rozgonyi and C. V. Shank (Materials Research Society, Pittsburgh, 1985).

[26]A. M. Malvezzi, H. Kurz, and N. Bloembergen, in *Energy Beam-Solid Interactions and Transient Thermal Processing* (Ref. 25).

[27]P. N. Saeta, Ph.D. thesis, Harvard University, 1991.

[28]A. Othonos, H. M. van Driel, J. F. Young, and P. J. Kelly, Solid-State Electron. **32**, 1573 (1989).

[29]A. Othonos, H. M. van Driel, J. F. Young, and P. J. Kelly, Phys. Rev. B **43**, 6682 (1991).

[30]J. K. Wang, Y. Siegal, C. Z. Lü, and E. Mazur, Opt. Commun. **91**, 77 (1992).

[31]Y. Siegal, Ph.D. thesis, Harvard University, 1994.

[32]The experimental results presented here show major changes in the dielectric constant following excitation by the pump beam. Since the penetration depth is determined by the dielectric constant, its value when the probe beam arrives at the sample depends on the strength of the excitation and on the pump-probe time delay.

[33]D. L. Greenaway and G. Harbeke, *Optical Properties and Band Structure of Semiconductors* (Pergamon, Oxford, 1968).

[34]R. F. Potter, in *Optical Properties of Solids,* edited by S. Nudelman and S. S. Mitra (Plenum, New York, 1969).

[35]Note that if the oscillator strength and the spectral width of an absorption peak are held fixed, then the height of the absorption peak increases as its resonant frequency decreases.

[36]D. H. Reitze, H. Ahn, and M. C. Downer, Phys. Rev. B **45**, 2677 (1992).

[37]The effect of the Drude contributions is not noticeable in the behavior of $\mathrm{Re}(\varepsilon)$ at 4.4 eV because the Drude term has a $1/\omega^2$ dependence and is therefore smaller by a factor of 4 at the higher photon energy. Also, the band-structure changes at low fluences have a large effect on $\mathrm{Re}(\varepsilon)$ at 4.4 eV than at 2.2 eV because of the larger slope at 4.4 eV of $\mathrm{Re}(\varepsilon)$ as a function of photon energy.

[38]E. J. Yoffa, Phys. Rev. B **21**, 2415 (1980).

[39]D. H. Kim, H. Ehrenreich, and E. Runge, Solid State Commun. **89**, 119 (1994).

[40]V. M. Glazov, S. N. Chizhevskaya, and N. N. Glagoleva, *Liquid Semiconductors* (Plenum, New York, 1969).

[41]W. Jank and J. Hafner, J. Non-Cryst. Solids **114**, 16 (1989).

[42]S. Froyen and M. L. Cohen, Phys. Rev. B **28**, 3258 (1983).

[43]J. A. Van Vechten, R. Tsu, and F. W. Saris, Phys. Lett. **74A**, 422 (1979).

[44]R. Biswas and V. Ambegoakar, Phys. Rev. B **26**, 1980 (1982).

[45]P. Stampfli and K. H. Bennemann, Phys. Rev. B **42**, 7163 (1990).

[46]G. E. Jellison and F. A. Modine, Phys. Rev. B **27**, 7466 (1983).

[47]J. P. Walter, R. R. L. Zucca, M. L. Cohen, and Y. R. Shen, Phys. Rev. Lett. **24**, 102 (1970).